UV–VIS Absorption and NIR-Stimulated Emission of Nd^{3+}: PVA Films

Amrutha K. Adiyodi, P. V. Jyothy, N. V. Unnikrishnan

School of Pure and Applied Physics, Mahatma Gandhi University, Kottayam 686560, India

Received 3 December 2007; accepted 27 December 2008
DOI 10.1002/app.29971
Published online 30 March 2009 in Wiley InterScience (www.interscience.wiley.com).

ABSTRACT: Neodymium-doped polyvinyl alcohol films were prepared and the optical properties of the films were investigated. By applying Judd–Ofelt theory, the Ω parameters were obtained from the absorption spectrum. Various radiative parameters like transition probability for each level (A_J), total transition probability (A_T), branching ratio (β_R), radiative lifetime (τ_{rad}), and absorption cross-section (σ_A) were calculated. The theoretically obtained branching ratio and integrated absorption cross-section are found to be greater for the transition $^4F_{3/2} \rightarrow {}^4I_{11/2}$. From the emission spectrum peaked at 1064-nm stimulated emission cross-section (σ_E), the line width ($\Delta\lambda_{eff}$) is calculated to be 6.21×10^{-21} cm^2 and 41 nm, respectively. Further the variation of the optical gain with the length of the film was studied and the slope efficiency ($\eta = 8.5\%$) was determined from laser measurements. These results clearly support the potentiality of the Nd^{3+}: polyvinyl alcohol films in realizing optical amplification and stimulated emission.
 J Appl Polym Sci 113: 887–895, 2009

Key words: rare earth; neodymium; polyvinyl alcohol; Judd–Ofelt parameters

INTRODUCTION

Polymers are considered good host materials for rare earth ions as they can be designed to yield a variety of bulk physical properties and they normally exhibit long-term stability and possess flexible reprocessability. They can be processed easily, which is an advantage in the fabrication of optical devices.[1] Rare earth ions have been widely used in silica glass based lasers and optical amplifiers. However, in recent years, rare earth ions-containing polymers have attracted much attention for their potential applications in luminescence devices, laser systems, and optical communication components.[2–5] Polymer hosts make it possible to incorporate rare earth ions in higher concentrations, preventing concentration quenching at higher concentrations.[6] Further, polyvinyl alcohol (PVA) films can be used as host matrices for transition metal elements, rare earth ions, dyes, nanoparticles, etc., which can be used for a wide range of applications in image storage, holography, laser applications, sensors, display applications, photovoltaic cells, etc.[7–10] In particular, the photo-electron paramagnetic resonance of Nd^{3+} ions in PVA films, the spectroscopic parameters of Sm^{3+} ions, and the photoacoustic studies of Sm^{3+} ions in PVA films have been reported.[11,12] The spectroscopic studies of Nd^{3+} in the polymer poly(methyl methacrylate) matrix have been reported but such works are relatively limited in PVA matrix. In view of these facts, we have attempted spectroscopic studies of Nd^{3+} ions in PVA matrix. The Judd–Ofelt theory has been widely used to estimate the radiative properties of the rare earth containing materials because the model provides reasonable values on an average. The Judd–Ofelt phenomenological parameters, Ω_2, Ω_4, and Ω_6, of doped material were obtained from the absorption spectrum. Based on the Judd–Ofelt theory,[13,14] the transition probabilities, fluorescence branching ratios, and radiative lifetime of Nd^{3+} doped PVA films were calculated. The radiative properties of the $^4F_{3/2} \rightarrow {}^4I_{11/2}$ transition indicate that it favors a potential laser transition. To ascertain the capability of the material in realizing optical amplification and laser action, we have also performed optical gain and stimulated emission measurements.

EXPERIMENTAL

Pure PVA film and doped ones with neodymium concentrations of 6, 7, 8, 9, and 10% by weight were grown by slow evaporation at room temperature.[15] The doped samples were designated as Samples A, B, C, D, and E, respectively. PVA was dissolved in double-distilled water and then heated on a hotplate for a few minutes. Subsequently the neodymium chloride dissolved in water was mixed with the PVA solution. Following the procedure reported elsewhere, Nd^{3+} ions were added in their nitrate or chloride form in solutions. It has been well

Correspondence to: N. V. Unnikrishnan (nvu50@yahoo.co.in).

established that the added amount would be intact in the matrix.[16–18] The solution, cast into a polypropylene dish, was kept at 50°C for 2 days. The films were peeled off from the polypropylene dish. These films were used for spectral investigations. The thickness of the films was measured by using a Prism Coupler (Metricon 2010, USA) at 633 nm and found to be 17 μm. The refractive index was also measured and the value was found to be 1.49. The absorption and fluorescence spectra were recorded by using the spectrophotometers Shimadzu-UVPC 2401 (Japan) and Shimadzu-RFPC-5301 (Japan), respectively. The thermogravimetric analysis (TGA, Japan) of the film was done by using a Shimadzu DTG-60. FTIR spectrophotometer was used for recording the IR spectra of the samples in the region of 4000–500 cm^{-1}. The optical gain experiments were done by using the L-L/2 method. For optical gain studies, cover glass slides of varying lengths were dipped horizontally in the Nd^{3+}/PVA solution in a Petri dish. These were allowed to cure in the oven for 2 days at 50°C and were taken out. The excess liquid at the top of the substrate was drained away on curing. This avoids ballooning of the films at the bottom side and ensures good adherence to the substrate. The thicknesses of the films were measured to be around 22 μm and the film lengths varied between 6 and 36 mm. The laser experiments were performed by 807-nm diode laser as the pump source and detection system was a combination of an InGaAs photodiode (Perkin-Elmer, USA), a linear amplifier, and a spectrum analyzer (Agilent 86142B spectrum analyzer, USA). The laser output energy was measured by using a power meter (407-A Spectra-Physics, USA).

THEORETICAL ANALYSIS

The theory of atomic spectra allows identification of definite J levels of $4f^3$ in the Nd^{3+} ion. A convenient way of representing the intensity of an absorption band is to measure the oscillator strength of the transition, which is found to be proportional to the area under the absorption line shapes. The oscillator strength (f) can be expressed in terms of the molar extinction coefficient (ε), and the energy of the transition in wave number (ν) by the relation.[19]

$$f_{\exp} = 4.32 \times 10^{-9} \int \varepsilon(\nu) d\nu \tag{1}$$

The absorption properties of rare earth ions are best distinguished in the context of the Judd–Ofelt theory.[20] In essence, the $4f \rightarrow 4f$ transitions of a rare earth ion can be described as a simple linear combination of the so-called J-O parameters $\Omega_\lambda(\lambda = 2, 4, 6)$. The coefficients of each linear combination of Ω_λ are independent of the host and are determined by the fundamental nature of the $4f$ wave functions and the particular transitions at hand.

According to J-O theory

$$f_{\text{ed}} = \frac{\nu}{(2J+1)} \left[\frac{8\pi^2 mc}{3h} \frac{(n^2+2)^2}{9n} \right] \sum_{\lambda=2,4,6} \Omega_\lambda \langle \psi J \| U^\lambda \| \psi' J' \rangle^2 \tag{2}$$

where (2J + 1) is the degeneracy of the ground state, ν is the mean energy of the $|\psi J\rangle \rightarrow |\psi' J'\rangle$ transition, U^λ is a unit tensor operator of rank λ, and Ω_λ's are known as J-O intensity parameters. Because of the electrostatic shielding of the $4f$ electrons by the closed 5p shell electrons, the matrix elements of the unit tensor operator between two energy manifolds in a given rare earth ion do not vary significantly when it is incorporated in different hosts. Therefore, the matrix element computed for the free ion may be used for further calculations in different media and are reported by Carnaal et al.[20] To obtain the accuracy of the intensity parameters obtained, the root-mean-squared deviations (δ_{rms}) are calculated using the relation $\delta_{\text{rms}} = \Sigma((f_{\exp} - f_{\text{cal}})^2/(N-M))^{(1/2)}$, where N is the number of levels fitted and M is the number of parameters determined. The bonding parameter (δ) is defined as $\delta = ((1-\bar{\beta})/(\bar{\beta})) \times 100$, where $\bar{\beta} = \sum_N \beta/N$ and $\beta = \nu_c/\nu_a$ (the nephelauxetic ratio), ν_c and ν_a are the energies of the corresponding transitions in the complex and aqua ion, respectively, and N refers to the number of levels used to compute $\bar{\beta}$ values. Depending on the environmental field, δ may be positive or negative indicating covalent or ionic bonding, respectively.[19]

Radiative transition parameters such as total radiative transition probability (A_T), radiative lifetime (τ_{rad}), and the fluorescence branching ratio (β_R) are calculated by using the known expressions.[19] The position of J levels of $4f^n$ in condensed matter is treated by the same techniques as for monatomic entities, but the probabilities of absorption and emission between J levels are entirely different. Radiative transition probabilities of the rare earths in polymers are composed mainly of the electric dipole contribution and to a much lesser extent by the magnetic dipole contribution. For rare earth ions, taking account of multiple terms splitting, its spontaneous radiative transition probability becomes

$$A_{JJ}^{\text{ed}} = \frac{64\pi^2 e^2 \upsilon^3}{3h(2J+1)} \left[\frac{n(n^2+2)^2}{9} \right] S_{\text{ed}} \tag{3}$$

where

$$S_{\text{ed}} = \sum_{\lambda=2,4,6} \Omega_\lambda \langle \psi J \| U^\lambda \| \psi' J' \rangle^2. \tag{4}$$

As the coefficients for spontaneous emission equal the reciprocal radiative relaxation time, we have

$$A^{ed}_{JJ'=}\tau^{-1}_{rad} \tag{5}$$

or

$$\tau_{rad} = \frac{1}{\sum_{J'} A_{JJ'}} \tag{6}$$

The position of the lines in absorption or emission spectra seems to be independent of the surroundings. Their intensity ratios vary strongly, indicating certain selection rules, which are reflected by the branching ratio. The relative amplitudes of the fluorescence transitions or fluorescence branching ratio are given by

$$\beta_{JJ'} = \frac{A_{JJ'}}{\sum_{J'} A_{JJ'}} \tag{7}$$

Branching ratio is the ratio of the radiative transition probability to the total radiative relaxation rate. It measures the percentage of emission for a given transition from a state with respect to all other transitions from this state. The integrated absorption cross-section or effective cross-section (σ_A) for stimulated emission is estimated by using the Fuchtbauer–Landenberg equation:

$$\sigma_A = \frac{A(\psi J)}{8\pi c n^2 \upsilon^2} \tag{8}$$

The effective cross-section, which is the stimulated cross-section integrated over the total band, gives a measure of the peak stimulated emission cross-section for transitions under the assumption that the bands do not contain sharp emission peaks. Knowing the radiative transition probability and effective fluorescence line width, the stimulated emission cross-section (σ_E) can be calculated by using the equation

$$\sigma_E = \frac{\lambda_p^4}{8\pi c n^2 \Delta\lambda_{eff}} A(\psi J, \psi' J') \tag{9}$$

where λ_p is the peak wavelength of the emission transition and $\Delta\lambda_{eff}$ is the effective band width of the emission transition.

RESULTS AND DISCUSSION

FTIR analysis

The FTIR spectra of the pure PVA and doped samples in the region 4000–500 cm^{-1} are shown in Figure 1(a) and those in the region 1000–500 cm^{-1} are shown in Figure 1(b). The spectrum exhibits band characteristics of stretching and bending vibrations of O—H, C—H, C=C, and C=O groups. The IR band positions of the samples and their assignments are shown in Table I. The FTIR spectrum clearly shows water content in the sample. Moreover the PVA sample has the tendency to absorb moisture from the atmosphere, which will again add to the intrinsic water content. In the low-frequency region the weak peak at 737 cm^{-1} band, which is absent in the pure PVA sample, is assigned to metal oxygen bond.[21]

Thermal analysis

Thermogravimetric curve is a plot of weight change versus temperature. The weight is plotted on the ordinate and temperature on the abscissa. PVA films

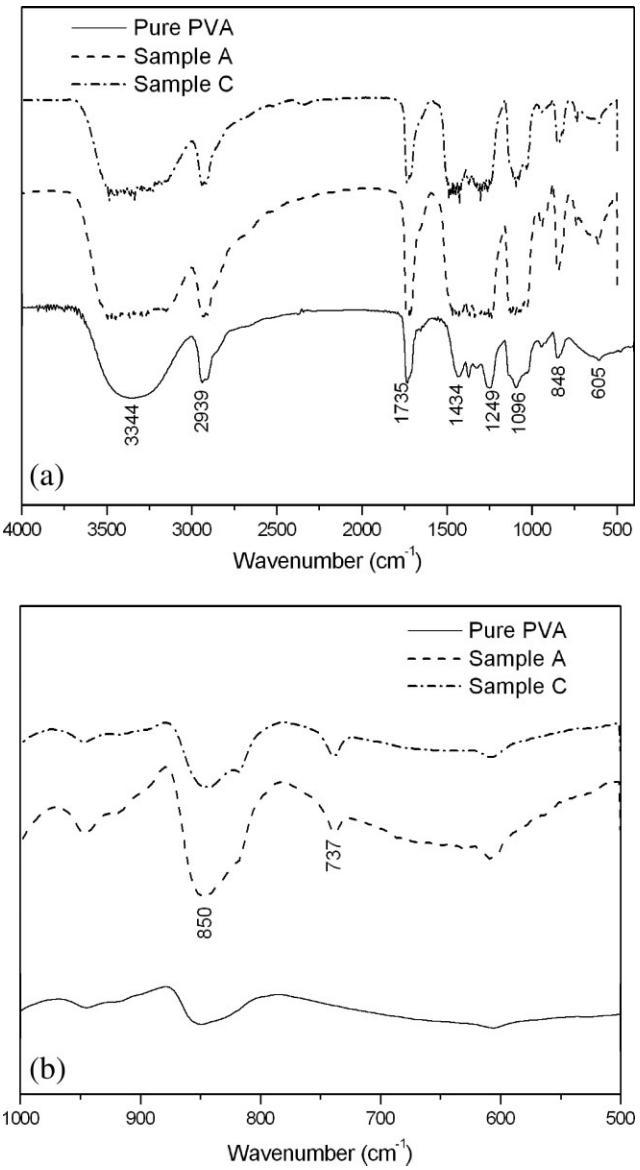

Figure 1 (a) FTIR spectra of PVA samples (pure PVA, Sample A (Nd^{3+} 6%/PVA) and Sample C (Nd^{3+} 8%/PVA)), (b) FTIR spectra of PVA samples (pure PVA, Sample A (Nd^{3+} 6%/PVA) and Sample C (Nd^{3+} 8%/PVA)).

TABLE I
FTIR Band Assignments of the PVA Samples

Vibrational frequency (cm^{-1})	Band assignment
3344	OH (stretching)
2939	CH_2 (stretching)
1735	C=O (stretching)
1434	CH_2 (bending)
1373	CH + OH
1326	CH + OH
1249	CH (stretching)
1095	CO (stretching)
945	CC (stretching)
848	CH_2 (stretching)
737	Metal-oxygen
605	OH (stretching)

are highly transparent in the visible range of wavelength, which may be utilized in transparent electronic devices. The thermal property of the PVA film was obtained by using TGA analysis. It was found that the degradation of the pure PVA film starts at around 300°C [Fig. 2(a)]. As a representative, the TGA/DTA curve of this Sample B is shown in Figure 2(b). From the figure it is clear that the addition of the rare earth ion causes the sample to degrade at a lower temperature. This tendency of degradation at around 200°C is also shown by all other samples. The degradation of polymers starts with free radical formations at weak bonds and/or chain ends, followed by their transfer to adjacent chains via interchain reactions. The shift to the lower temperature may be due to the formation of nonbridging oxygen from PVA by the incorporation of the rare earth ions and the bonds in the PVA break at a lower temperature. This is well supported by the metal ion oxygen bonding observed in the FTIR spectrum.

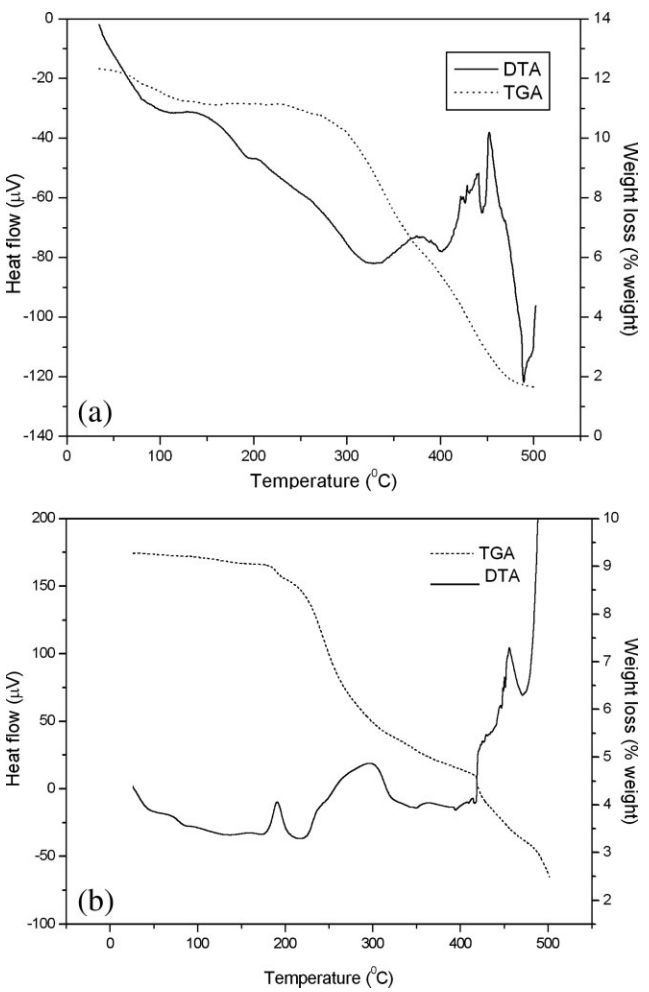

Figure 2 (a) TGA/DTA curve of pure PVA sample; (b) TGA/DTA curve for Sample B.

Absorption studies

The absorption spectra of pure PVA film and doped films are shown in Figures 3 and 4, respectively. The pure sample shows a weak band at 280 nm. This peak is assigned to the carbonyl groups associated with ethylene unsaturation, which indicates the presence of conjugated double bonds of polyenes. The major mechanism for transitions in rare earth ions is induced electric dipole arising from the very weak mixing of the order of magnitude of the ground state $4f^n$ wave function with functions of the opposite parity. The ground state of the Nd^{3+} ion is $^4I_{9/2}$ and the absorption bands arise due to transitions from this level to various excited levels. The spectral lines observed are assigned for different excited states $^2H_{11/2}$, $^4G_{9/2}$, $^4G_{7/2}$, $^4G_{5/2}$, $^4S_{3/2}$, $^4F_{5/2}$ and $^4F_{3/2}$.[20] The absorption spectra of doped PVA for different wt% of neodymium ions follow a linear relationship with Nd^{3+} concentrations. The intensity of the bands is found to increase with the doping level of Nd^{3+} in the PVA matrix.

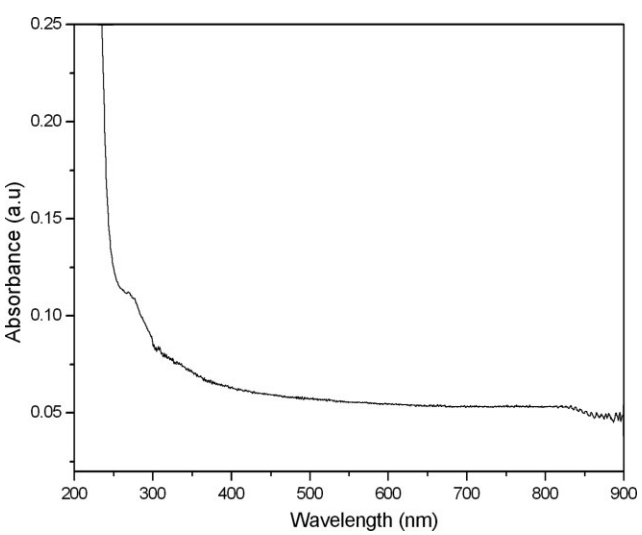

Figure 3 Absorption spectrum of pure PVA film.

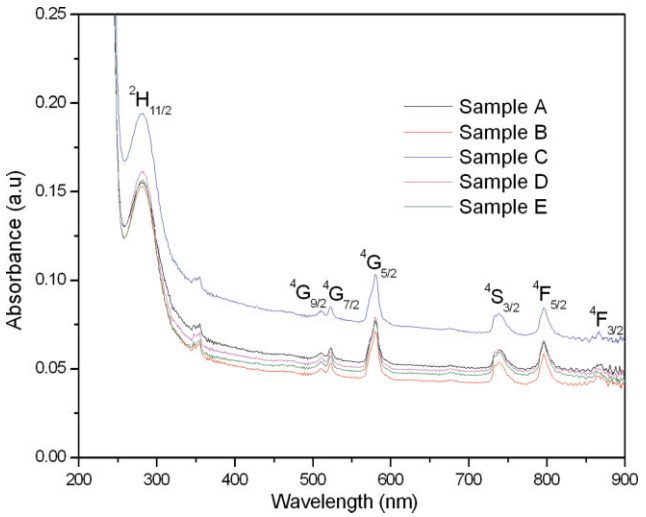

Figure 4 Absorption spectra of $Nd3^+$ doped PVA films. [Color figure can be viewed in the online issue, which is available at www.interscience.wiley.com.]

For most practical purposes the oscillator strengths and the connected radiative transition probabilities obtained from the absorption spectra correspond to some average values due to the total number of sites. A small shift of the free ion levels to lower energies can be observed as a result of the covalency between the rare earth and the polymer matrix. Experimentally determined oscillator strengths and the calculated oscillator strengths are tabulated in Table II. The values are comparable with that obtained for phosphate and borate glasses.[22,23] From the table it is clear that the higher value of oscillator strength is obtained for the transition $^4I_{9/2} \rightarrow {}^4G_{5/2}$. Because it is hypersensitive in nature, any local structural change may sharply affect the value. In some matrices, because of its very large value compared to the other transitions, it is excluded from the calculation of J-O parameters. The root-mean-squared deviations in determining oscillator strength are also given in Table II and these values are comparable with other Nd^{3+} systems.[22–24]

The J-O parameters of Nd^{3+} in PVA matrices for the five samples are given in Table III. According to J-O theory, the oscillator strength is found to be functions of the three J-O parameters and varies from site to site. The J-O parameters are functions of crystal field parameters, intraconfigurational radial integral, and energy separation of the $4f^N$ and opposite parity configuration. Hence these parameters are dependent on the oscillator strengths and are found to vary from site to site. Here the parameters show a tendency of $\Omega_6 > \Omega_2 > \Omega_4$ as seen in heavy metal fluoride glasses. There is no general tendency in the values of Ω_λ parameters; it may be different from matrix to matrix.[23] The Ω_2 and Ω_6 values are seen to be increasing with the concentration (Table III).

For Nd^{3+} the intensity of $^4I_{9/2} \rightarrow {}^4G_{5/2}$ transition is the principal determining factor for Ω_2.[23] The increase in covalency (R-O covalency) is manifested directly in the increase of the parameter Ω_2. The parameter Ω_2 is related to the covalency and/or local structural changes in the vicinity of the Nd^{3+} ion (short-range effect).[25] Covalent bonding has the effect of lowering the electronic levels of the free ion due to the nephelauxetic effect and the value of Ω_2 gets strongly enhanced. A large value of Ω_2 intensity parameter is an indication of high covalence of the metal–ligand bonds. High covalent bonding provides greater Ω_2 values, which indicates lower symmetry around the rare earth ion in the host. These parameters in turn determine the electric dipole and magnetic dipole line strengths of a transition. The bonding parameter (δ) obtained is also given in Table III and found to be negative, which indicates the presence of ionic bonds.

Once the Ω_λ quantities have been determined, they can subsequently be utilized to calculate the properties of fluorescent transitions from the $^4F_{3/2}$ level that has not been experimentally measured, including the radiative lifetime. The values of the radiative transition probability (A_J), total radiative transition probability (A_T), radiative lifetime (τ_{rad}), fluorescence branching ratio (β_R), and the integrated absorption cross-section for stimulated emission (σ_A) are given in Table IV.

Jorgensen and Reisfeld[26] related the intensity parameters Ω_4 and Ω_6 to the rigidity of various hosts such as crystals, glasses, solutions, and vapors. Takabe et al.[27] suggested that the ionic packing ratio is related to the spontaneous emission probabilities

TABLE II
Experimental and Calculated Values of Oscillator Strength (10^{-6})

Transition from $^4I_{9/2}$	Sample A		Sample B		Sample C		Sample D		Sample E	
	f_{exp}	f_{cal}	f_{exp}	f_{cal}	f_{exp}	f_{cal}	f_{exp}	f_{cal}	f_{exp}	f_{cal}
$^4G_{9/2}$	0.078	0.07	0.095	0.15	0.13	0.16	0.10	0.16	0.052	0.18
$^4G_{7/2}$	0.091	0.21	0.12	0.29	0.14	0.317	0.12	0.31	0.14	0.37
$^4G_{5/2}$	1.0	1.01	1.4	1.39	1.5	1.52	1.5	1.52	1.6	1.58
$^4S_{3/2}$	0.59	0.635	0.89	0.95	0.83	0.89	0.99	1.06	0.92	1.0
$^4F_{5/2}$	0.64	0.58	0.95	0.86	0.91	0.83	1.0	0.94	1.1	0.95
RMS	0.14×10^{-6}		0.2×10^{-6}		0.18×10^{-6}		0.21×10^{-6}		0.29×10^{-6}	

TABLE III
J-O Parameters of the Samples

Sample	JO parameters ($\times 10^{-20}$ cm^2) Ω_2	Ω_4	Ω_6	Q-factor	Order	Bonding parameter
A	0.38	0.092	0.74	0.12	$\Omega_6 > \Omega_2 > \Omega_4$	−0.057
B	0.52	0.096	1.1	0.087	$\Omega_6 > \Omega_2 > \Omega_4$	−0.11
C	0.56	0.16	1.03	0.152	$\Omega_6 > \Omega_2 > \Omega_4$	−0.11
D	0.56	0.05	1.25	0.037	$\Omega_6 > \Omega_2 > \Omega_4$	−0.08
E	0.54	0.23	1.16	0.197	$\Omega_6 > \Omega_2 > \Omega_4$	−0.19

that are determined by the intensity parameters Ω_4 and Ω_6 and it correlates with the rigidity of the polymer hosts and the covalency of the rare earth ion sites. In the Nd^{3+} ion the level $^4F_{3/2}$ fluoresces in four bands centered at approximately 880, 1060, 1350, and 1800 nm corresponding to $^4I_{9/2}$, $^4I_{11/2}$, $^4I_{13/2}$, and $^4I_{15/2}$, respectively. Because the matrix element $\langle {}^4F_{3/2}$ IIU^{2}II $^4I_J\rangle$ is zero, the Ω_2 parameter will not have any effect on the stimulated emission parameters of Nd^{3+} ions. The luminescence branching ratio can then be represented as dependent only on one parameter, Ω_4/Ω_6, which is usually known as the quality factor (Q). The Q values are tabulated in Table III. The branching ratio (β_R) for the four transitions has been plotted as a function of Q-factor for the four laser transitions (Fig. 5). It is clear that the maximum possible value of β for $^4F_{3/2} \rightarrow {}^4I_{11/2}$ is about 0.66 (for $Q = 0$) and for the additional $^4F_{3/2} \rightarrow {}^4I_{13/2}$ channel is about 0.15. Maximum luminescence can be observed for the $^4F_{3/2} \rightarrow {}^4I_{9/2}$ transition for very high values of Q. Another way of defining the quality factor is to take luminescence intensities of Nd^{3+} ion for the different $^4F_{3/2} \rightarrow {}^4I_J$ emission channels. The variation of the intermultiplet ($\beta_{11/2}$, $\beta_{13/2}$) branching ratio with spectroscopic quality factor is shown in Figure 6. This variation shows a linear dependence on Q-factor. The changes in the local environment can vary the radiative lifetime of the $^4F_{3/2}$ level in a substantial manner, which clearly indicates that the lifetime is a matrix-dependent parameter.

Fluorescence studies

A typical emission spectrum of Sample C is shown in Figure 7. The ions excited to one of the higher states relax via radiative or multiphonon transition to the level $^4F_{3/2}$. In fact this level $^4F_{3/2}$ fluoresces in four bands and the main peak, with an appreciable intensity, is at 1064 nm, corresponding to $^4F_{3/2} \rightarrow {}^4I_{11/2}$ transition and therefore only this peak is shown in the figure. From Table IV it is clear that other levels have a very low branching ratio compared to the $^4F_{3/2} \rightarrow {}^4I_{11/2}$ transition. Moreover, it is known that the water content of the matrices shifts the emission spectrum as compared to the isolated Nd^{3+} ions and quenches the fluorescence. The presence of water content is confirmed from the OH bands in the FTIR spectrum. This may affect or quench the other low-intensity transitions appreciably. It is experimentally observed that the fluorescence intensity attains its maximum value for Sample C (Nd^{3+} 8 wt %) and then deceases with increasing concentration. This quenching behavior of fluorescence can be explained by the processes,

TABLE IV
Different Radiative Parameters of the Samples

Samples	Transition from $^4F_{3/2}$	Wave no. υ (cm^{-1})	S_{ed} 10^{-20} (cm^2)	A_J (s^{-1})	A_T (s^{-1})	τ_{rad} (ms)	β_R (%)	σ_A 10^{-20} (cm^2)
Sample A	$^4I_{15/2}$	5450	0.02	1.89	247.37	4.01	0.77	3.6
	$^4I_{13/2}$	7520	0.16	37.75			15.26	38.33
	$^4I_{11/2}$	9520	0.31	153.42			62.01	97.22
	$^4I_{9/2}$	11,530	0.062	54.31			21.95	23.46
Sample B	$^4I_{15/2}$	5450	0.031	2.84	359.84	2.77	0.79	5.5
	$^4I_{13/2}$	7520	0.24	56.61			15.73	57.49
	$^4I_{11/2}$	9520	0.47	227.20			63.14	143.98
	$^4I_{9/2}$	11,530	0.084	73.18			20.33	31.61
Sample C	$^4I_{15/2}$	5450	0.029	2.43	324.61	3.08	0.75	4.7
	$^4I_{13/2}$	7520	0.22	48.43			14.92	49.19
	$^4I_{11/2}$	9520	0.44	198.70			61.21	125.92
	$^4I_{9/2}$	11,530	0.094	75.04			23.11	32.42
Sample D	$^4I_{15/2}$	5450	0.035	2.95	357.1	2.8	0.83	5.69
	$^4I_{13/2}$	7520	0.265	58.6			16.41	59.5
	$^4I_{11/2}$	9520	0.515	231.23			64.75	146.53
	$^4I_{9/2}$	11,530	0.081	64.32			18.01	27.78
Sample E	$^4I_{15/2}$	5450	0.033	2.73	377.5	2.6	0.72	5.29
	$^4I_{13/2}$	7520	0.25	54.51			14.41	55.27
	$^4I_{11/2}$	9520	0.51	226.55			60.01	143.57
	$^4I_{9/2}$	11,530	0.118	93.79			20.84	40.52

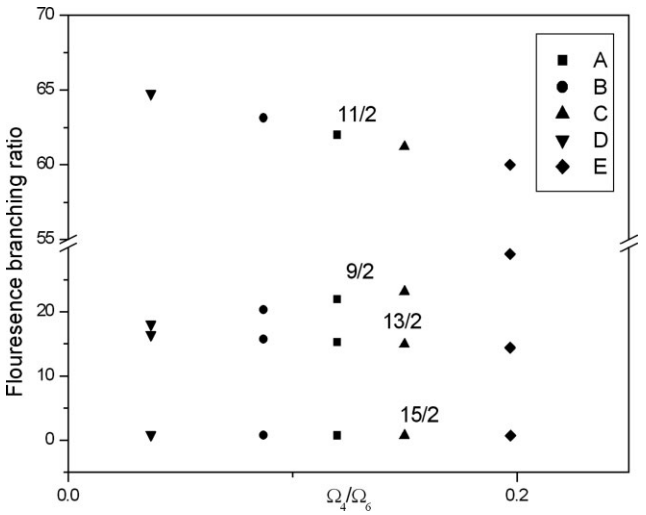

Figure 5 Variation of branching ratios with *Q*-factor for different samples.

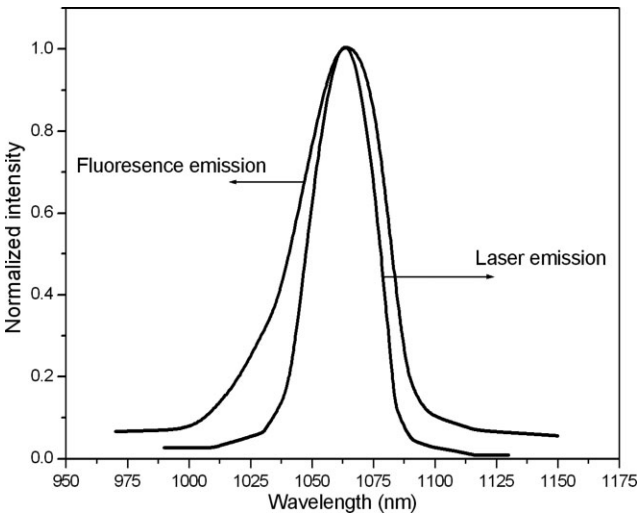

Figure 7 Fluorescence and laser emission spectra of Sample C.

namely, (1) concentration quenching, (2) cross relaxation, and (3) radiation trapping. Concentration quenching is related to the interaction of an excited Nd^{3+} ion with a coupled unexcited neighbor so that the first makes a transition from $^4F_{3/2}$ to $^4I_{13/2}$ or $^4I_{11/2}$. At the same time the second one (coupled unexcited) makes a transition from $^4I_{9/2}$ to $^4I_{15/2}$. Both then decay nonradiatively back to $^4I_{9/2}$ ground state. The cross relaxation is the case in which an excited Nd^{3+} ion makes a transition from $^4F_{3/2}$ to $^4I_{9/2}$, while a coupled unexcited neighbor makes the reverse transition. Radiation trapping involves the same initial and final states of the two-ion system with energy being transferred by photon emission and capture.

The theoretically obtained branching ratio and integrated absorption cross-section for the $^4F_{3/2} \rightarrow$ $^4I_{11/2}$ transition is higher than those for other transitions. From eq. (9) it is clear that the stimulated emission cross-section σ_E is dependent on the Ω parameters and $\Delta\lambda_{eff}$; both are composition dependent. Thus to obtain a large value of σ_E for the transition, it is necessary to maximize both Ω_4 and Ω_6. The values of σ_E and the $\Delta\lambda_{eff}$ are 6.13×10^{-21} cm^2 and 41 nm, respectively. The stimulated emission parameters obtained for the PVA matrix compare well with certain glass matrices like silicate, borate,[23] polymer optical fiber, and polystyrene sulfonate films.[28]

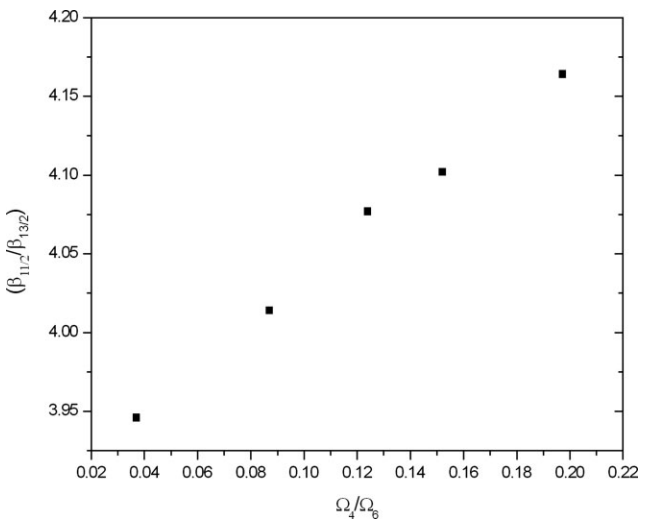

Figure 6 Variation of intermultiplet branching ratio with quality factor.

Optical gain and laser studies

The optical gain of the sample is measured by using amplified spontaneous emission technique. Here we used the *L*-*L*/2 method for the gain measurements.[29] In this technique the length of the gain region may be varied from *L* to *L*/2 by blocking off one-half of the pumping beam by a shutter. The experimental setup for measuring the gain of the samples is given in Figure 8. Here we measure the emission from a full and a half length of the sample. The gain

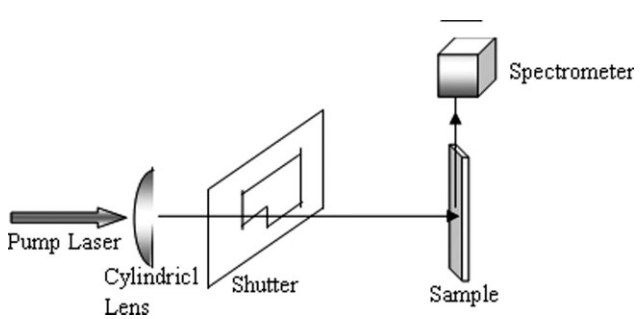

Figure 8 Experimental setup for gain measurements.

coefficient, α, can be computed from the ratio of the resultant signals I_L and $I_{L/2}$ and is given by

$$\alpha = \frac{2}{L}\ln\left(\left(\frac{I_L}{I_{L/2}}\right) - 1\right) \quad (10)$$

The relationship between the gain coefficient and the optical gain is given by the equation,

$$G = e^{-\alpha L}. \quad (11)$$

Because Sample C (8 wt % Nd^{3+}) has been identified as the optimal one with maximum fluorescence intensity, we have chosen the same for optical gain and laser studies. The optical gain obtained for Sample C is 2.8 dB for a pumped length of 6 mm. The low value of gain is attributed to the small length of the gain region. Nevertheless, larger lengths of the gain region can yield high gain. To prove this, we have examined the variation of the optical gain for other lengths of the pump region. The gain values obtained are 6.2, 9.7, 12.5, 8.6, and 4.4 dB for 12-, 18-, 24-, 30-, and 36-mm lengths, respectively. It is inferred from the results that the amplified emission signal growth is followed by a decline. The total gain dominates over the combined loss effects (Fresnal losses, propagation losses, and absorption and reabsorption losses) of the PVA host up to a length of 24 mm. For lengths above 24 mm, the combined loss effects dominate over the amplified emission, causing a decrease of the output signal.

Because Nd^{3+} has an absorption peak around 800 nm, for laser emission studies the sample coated on the glass substrate is transversely pumped by the 807-nm diode laser.

The pump beam was focused onto the sample by a cylindrical lens. The size of the line-focused laser beam was 10 mm long and 0.2 mm wide. The output from the transverse laser emission was monitored by a combination of an InGaAs photodiode, a linear amplifier, and a spectrum analyzer (Fig. 9). Here no resonator was used, because the optical feedback is

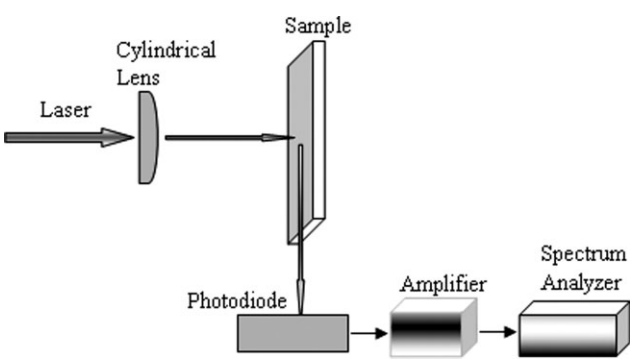

Figure 9 Experimental setup for laser emission from the sample.

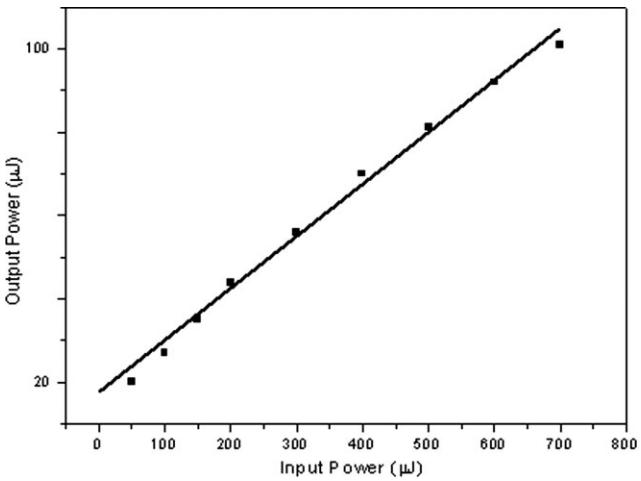

Figure 10 Input–output characteristics of Sample C.

provided by Fresnel reflectivity at the polymer–air interface at both ends. The input–output characteristic of Sample C is shown in Figure 10. The average slope efficiency (η) obtained is around 8.5%.

The normalized fluorescence spectrum and the laser emission spectrum for Sample C are shown in Figure 7. The spectral narrowing of the laser emission spectrum is clearly evident in this figure. The laser line width is estimated to be $\Delta\lambda_L = 31$ nm, which is clearly less than the fluorescence line width ($\Delta\lambda_{eff}$). Because a significant part of the pump energy is transmitted through the sample, the efficiency in fact is evaluated as the ratio of the output energy to the absorbed energy.

From these studies it is inferred that the transition $^4F_{3/2} \rightarrow {}^4I_{11/2}$ can be utilized for optical amplification in Nd^{3+} doped PVA films. Some of the major advantages attributed to polymers in the context of polymers doped with rare earth ions are (i) the rare earth ions doped polymer matrix shows higher covalent bonding, (ii) such systems are ideal candidates for optical image storage, (iii) a hologram could be written easily at a wavelength corresponding to the absorption peaks of the rare earth ions, and (iv) they can be processed easily and exhibit better long-term photostability.

CONCLUSION

PVA samples with various Nd^{3+} concentrations were prepared and characterized. The thermal analysis shows that the degradation of the sample starts at 300°C. The FTIR analysis has been employed to ascertain the various molecular vibrations of the sample. It shows the presence of hydroxyl content within the sample. Even at 300°C or above it is extremely difficult to remove all the residual OH content, which acts as fluorescence quenchers. Heat

treatment at high temperature may reduce the water content but, on the other hand, may result in the complete degradation of the sample. The absorption spectra and the Judd–Ofelt analysis yielded various spectroscopic parameters. The J-O parameters specifically relevant to the fluorescence efficiency have been evaluated for various concentrations. The various important spectral parameters were obtained from the absorption spectrum such as radiative lifetime, transition probability, branching ratio, and absorption cross-section. The transition $^4F_{3/2} \rightarrow {}^4I_{11/2}$ has been identified as the one that yields the maximum fluorescence emission. The variation of the optical gain values with the pumped length of the film gives a maximum gain value of 12.5 dB for a pump length of 24 mm. The laser experiments yielded a slope efficiency of $\sim$ 8.5%. The low overall laser output energy by transverse pumping is mainly due to the low absorption pump energy by the films. Thus the evaluation of the radiative properties, optical gain, and stimulated emission characteristics indicate that Nd^{3+} doped PVA is a promising candidate for making polymer-based optically active devices.

We are thankful to the referees for a critical reading of the manuscript and many useful suggestions.

References

1. Ma, H.; Jen, A. K. Y.; Dalton, L. R. Adv Mater 2002, 14, 1339.
2. Koeppen, C.; Yamada, S.; Jiang, G.; Garito, A. F.; Dalton, L. R. J Opt Soc Am B 1997, 14, 155.
3. Kuriki, K.; Koike, Y.; Okamoto, Y. Chem Rev 2002, 102, 2347.
4. Liang, H.; Zhang, Q.; Zheng, Z.; Ming, H.; Li, Z.; Xie, J.; Chen, B.; Zhao, H. Opt Lett 2004, 29, 477.
5. Slooff, L. H.; de Dood, M. J. A.; van Blaaderen, A.; Polman, A. Appl Phys Lett 2000, 76, 3682.
6. Kobayashi, T.; Kurki, K.; Imai, N.; Tamura, T.; Sasaki, K.; Koike, Y.; Okamoto, Y. Proc SPIE 1999, 206, 3623.
7. Changkakoti, R.; Manivannan, G.; Singh, A.; Lessard, R. A. Opt Eng 1993, 32, 2240.
8. Yap, S. S.; Siew, W. O.; Tou, T. Y.; Ng, S. W. Appl Opt 2002, 41, 1725.
9. Thomas, J.; Kumar, G. A.; Unnikrishnan, N. V.; Nampoori, V. P. N.; Vllabhan, C. P. G. Mater Lett 2000, 44, 275.
10. Karthikeyan, B. Phys B 2005, 364, 328.
11. Mumar, M.; Babu, Y.; Dhobale, A. R.; Kadam, R. M.; Sastry, M. D. J Polym Sci Part B: Polym Phys 1997, 35, 187.
12. Adiyodi, A. K.; Jyothy, P. V.; Toney, T. F.; Jose, G.; Unnikrishnan, N. V. Optoelectron Adv Mater: Rapid Commun 2007, 1, 281.
13. Judd, B. R. Phys Rev 1962, 127, 750.
14. Ofelt, G. S. J Chem Phys 1962, 37, 511.
15. Selim, M. S.; Seoudi, R.; Shabak, A. A. Mater Lett 2005, 59, 2650.
16. Fan, X. P.; Wang, M. Q.; Xiong, G. H. Mater Sci Eng B 1993, 21, 55.
17. Nogami, M.; Nagakura, T.; Hayakawa, T. J Phys: Condens Matter 1999, 11, 335.
18. Nogami, M.; Nagakura, T.; Hayakawa, T.; Sakai, T. Chem Mater 1998, 10, 3991.
19. Jose, G.; Thomas, V.; Fernandez, T. T.; Amrutha, K. A.; Joseph, C.; Ittyachan, M. A.; Unnikrishnan, N. V. Phys B 2005, 357, 270.
20. Carnaal, W. T.; Fields, P. R.; Rajnak, K. J Chem Phys 1968, 49, 4424.
21. Duhan, S.; Aghamkar, P. Acta Phys Pol A 2008, 113, 1671.
22. Kumar, G. A.; Biju, P. R.; Unnikrishnan, N. V. Phys Chem Glasses 1999, 40, 219.
23. Kumar, G. A.; Biju, P. R.; Venugopal, C.; Unnikrishnan, N. V. J Non-Cryst Solids 1997, 221, 47.
24. Liang, H.; Zheng, Z.; Zhang, Q.; Ming, H.; Chen, B. Phys Status Solidi B 2004, 5, 1149.
25. Saisudha, M. B.; Ramakrishna, J. Phys Rev B 1996, 53, 6186.
26. Jorgensen, C. K.; Reisfeld, R. J Less-Common Met 1983, 93, 107.
27. Takabe, H.; Keji, M.; Izumitani, T. J Non-Cryst Solids 1994, 178, 58.
28. Silva, M. C.; Cristovan, F. H.; Nascimento, C. M.; Bell, M. J. V.; Cruz, W. O.; Marletta, A. J Non-Cryst Solids 2006, 352, 5296.
29. Fabeni, P.; Linari, R.; Pazzi, G. P.; Ranfagni, A. Appl Opt 1987, 26, 5317.